A novel biomarker-based proxy for the spring phytoplankton bloom in Arctic and sub-arctic settings – HBI T$_{25}$

Simon T. Belt [a,*], Lukas Smik [a], Denizcan Köseoğlu [a], Jochen Knies [b,c], Katrine Husum [d]

[a] *Biogeochemistry Research Centre, School of Geography, Earth and Environmental Sciences, Plymouth University, Plymouth, PL4 8AA, UK*
[b] *CAGE – Centre for Arctic Gas Hydrate, Environment and Climate, Department of Geosciences, UiT The Arctic University of Norway, 9037 Tromsø, Norway*
[c] *Geological Survey of Norway, N-7491, Trondheim, Norway*
[d] *Norwegian Polar Institute, Fram Centre, NO-9296 Tromsø, Norway*

ABSTRACT

The spring phytoplankton bloom is a characteristic feature of mid-high latitudes in modern times, but can be challenging to identify in palaeo records. In the current study, we investigated the absolute and relative distributions of two diatom-derived tri-unsaturated highly branched isoprenoid (HBI) lipids, at least one of which has previously been suggested to be a possible proxy for the productive region of the marginal ice zone (MIZ) in the Polar Regions. Based on a comparison of their distributions in surface sediments from the Barents Sea and neighbouring regions with a range of oceanographic parameters, we identify, via principal component analysis, a strong association between the relative proportion of the two HBIs and satellite-derived spring chlorophyll *a* (chl *a*) concentration. Further, based on agglomerative hierarchical clustering, we identify two clusters of HBI biomarker ratios and spring chl *a* together with a potential threshold biomarker ratio (termed HBI TR$_{25}$) for the spring phytoplankton bloom. A modified version of HBI TR$_{25}$ (i.e. HBI T$_{25}$) provides a potentially more straightforward binary measure of the spring phytoplankton bloom. Analysis of HBI TR$_{25}$ and HBI T$_{25}$ values in a series of short (spanning recent centuries) and long (Holocene) sediment cores from the region provides an initial evaluation of the applicability of this novel proxy in the palaeo record. Outcomes are mainly consistent with the findings from the surface sediments and with other proxy-based reconstructions, including estimates of past sea ice cover, which is well-known to influence primary production in the region. Indeed, we suggest that the new HBI T$_{25}$ phytoplankton bloom proxy may also represent an important new tool for characterising the MIZ in palaeo records, especially when used alongside well-established sea ice proxies, such as IP$_{25}$ and PIP$_{25}$. Despite the largely empirical nature of the study, we also provide a possible explanation for the observed biomarker ratio-chl *a* relationship. Thus, a previous laboratory investigation showed that the distributions of the same two HBIs analysed herein in their likely source (viz. *Rhizosolenia setigera*) was strongly influenced by culture temperature and growth rate. Confirmation of the generality of our findings and of the causal relationship between HBI T$_{25}$ and the spring phytoplankton bloom will, however, require further laboratory- and field-based studies in the future.

1. Introduction

The spring phytoplankton bloom is a particularly characteristic and important feature of mid- to high-latitude settings in the northern hemisphere (Mahadevan et al., 2012 and references cited therein). Relatively high photosynthetic light intensity combined with eddy-driven stratification and increased nutrient levels following winter vertical mixing, provide the necessary stimuli and growth conditions for rapid phytoplankton development, such that growth rates can outcompete those of grazing. As a consequence, phytoplankton blooms can contribute significantly to global fixing of atmospheric carbon and its subsequent export from surface waters. High phytoplankton productivity is also critical for the development and maintenance of primary consumers and higher trophic level marine ecosystems, more generally (Legendre, 1990; Søreide et al., 2010; Wassman et al., 2006).

As a response to recent and rapid climate change in the Arctic and sub-arctic regions, and a reduction in sea ice cover, in particular, various changes to phytoplankton dynamics are beginning to emerge. For example, spring blooms in sub/low-Arctic regions are developing earlier due to a more rapid retreat of the productive
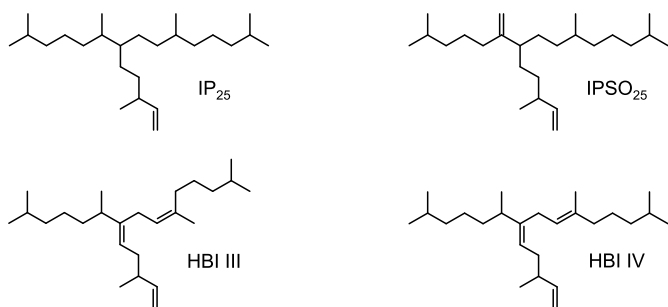
Fig. 1. Structures of highly branched isoprenoid (HBI) biomarkers investigated in the current study.

marginal ice zone (MIZ), and the productive period, in general, is lengthening due to both earlier ice retreat in late winter/spring and later freeze-up in late summer/autumn (Renaut et al., 2018 and references cited therein). Further, in ice-marginal locations such as the Barents Sea and the Kara Sea, which exhibit greatest sensitivity to modern sea ice change (Lind et al., 2018 and references cited therein), northward expansion of phytoplankton blooms (Renaut et al., 2018) and increased prevalence of under-ice phytoplankton blooms have been reported, which likely result from thinning of sea ice, reduced precipitation (snow) and an increase in the frequency of open-water leads between ice floes (Arrigo et al., 2012).

Although such observations and possible attributions can be made through contemporary in situ measurements, deducing the same within palaeo records is much less straightforward to achieve, partly due to the challenge of finding suitable proxy measures, especially of the spring bloom, uniquely. Several proxy methods for estimating past changes in overall marine primary productivity exist (see Ragueneau et al., 2000 for an overview), including those based on elemental composition, stable isotopes and microfossil assemblages, although, as with all proxies, each have their limitations. Biogenic silica can potentially more accurately reflect the dominance of diatoms and radiolarians commonly associated with the spring bloom, although dissolution and often poor sedimentary preservation are limitations (Ragueneau et al., 2000). Similarly, the accumulation rates of certain benthic foraminifera, known to be opportunistic consumers of fresh phytodetritus and thus a potential proxy measure of the spring bloom, may be negatively influenced by significant carbonate dissolution, especially in high latitude locations (Polyak et al., 2013; Seidenkrantz, 2013).

Certain source-specific lipids in marine sediments from high latitude settings have emerged as useful paleoceanographic proxies over the last decade or so. For example, the mono- and di-unsaturated highly branched isoprenoid (HBI) biomarkers IP_{25} and $IPSO_{25}$ (Fig. 1) have been proposed as binary measures of seasonal sea ice in the Arctic and Antarctic, respectively, a signature based on their selective production by certain sea ice-associated (i.e. sympagic) diatoms only (see Belt, 2018 for a recent review). Further, by considering the variable concentrations of IP_{25} and $IPSO_{25}$ alongside those of some open-water (i.e. pelagic) biomarkers, either individually or in the form of the so-called PIP_{25} index (Müller et al., 2011), more semi-quantitative estimates of sea ice conditions have been proposed (Belt, 2018).

In some recent studies, a tri-unsaturated HBI lipid biomarker (often referred to as HBI III; Fig. 1) has been suggested to represent a suitable open-water counterpart to IP_{25} and $IPSO_{25}$, partly due to its source-specific production by certain pelagic diatoms (Belt, 2018). Interestingly, based on water column and sediment data from the Arctic and the Antarctic, it has been suggested that HBI III might represent a useful proxy for the MIZ, with its elevated abundance in such regions (Belt et al., 2015; Schmidt et al., 2018; Belt, 2018; Bai et al., 2019) reflecting the more general feature of higher productivity commonly observed along the retreating ice

margin (Sakshaug et al., 2009; Wassmann et al., 2006). More generally, however, the establishment of a robust proxy for the MIZ remains an interesting research challenge.

Despite these previous reports, there have been no dedicated studies aimed at identifying any quantitative relationship(s) between HBI III and other well-recognised measures of primary production such as chlorophyll *a* (chl *a*) or indeed any other oceanographic feature. In the current study, we therefore compared the distribution of HBI III in ca. 200 surface sediments with a range of modern-day oceanographic parameters, including sea surface temperature, salinity, water depth, sea ice concentration, photosynthetically active radiation (PAR) and chl *a*. Here, we focus on the Barents Sea and neighbouring regions on the basis of well-documented and contrasting spring bloom dynamics, together with the availability of suitable surface and downcore sediment material. We also considered biomarker-based estimates of spring sea ice concentration (SpSIC; Smik et al., 2016) due to its influence over seasonal phytoplankton dynamics, and the distribution of a geometric isomer of HBI III (HBI IV; Fig. 1), not least because HBIs III and IV are often co-produced by certain common diatoms (e.g. *Rhizosolenia setigera*; Rowland et al., 2001), with HBI IV having been shown recently to be a useful predictor of sea ice classification in the Barents Sea when used alongside IP_{25} (Köseoğlu et al., 2018a).

Having identified a strong relationship between the relative proportions of HBIs III and IV (but not the individual biomarkers) and spring chl *a*, but no other measured parameter, we then measured the same relative biomarker distribution in a series of short cores spanning recent centuries and longer (early-late Holocene) downcore records from the region. Our findings suggest that the proportion of HBIs III and IV in marine archives may provide a proxy measure of the past occurrence (or otherwise) of the spring phytoplankton bloom, at least for the Barents Sea and neighbouring regions. On the basis of an earlier laboratory investigation into the distributions of HBIs (including III and IV) in the cosmopolitan pelagic diatom *R. setigera*, we also suggest a possible origin of the proxy relationship between HBIs III and IV, and the spring phytoplankton bloom.

2. Regional setting

Detailed descriptions of Barents Sea oceanography can be found in Loeng (1991). In brief, the Barents Sea is characterised by three distinct water masses (Fig. 2a): northward inflow of warm and saline Atlantic Water (AW) via the North Atlantic Current (NAC), which continues further north as the North Cape Current (NCaC) and the West Spitsbergen Current (WSC), fresher and colder Arctic Water (ArW) flowing southwest via the East Spitsbergen Current (ESC) and the Persey Current (PC), and brackish coastal water topographically steered along the Norwegian coast by the Norwegian Coastal Current (NCC) (Sakshaug et al., 2009). The northern region of the Barents Sea also experiences seasonal sea ice cover, reaching its maximum extent in March–April; however, inter-annual fluctuations can be large due to variable inflow of AW (Smedsrud et al., 2013). Overall, sea ice in the Barents Sea has decreased by >50% in the last 40 yr or so (Fetterer et al., 2016), a negative trend that has likely existed since 1850 AD (Divine and Dick, 2006). The region is almost entirely ice-free at the September sea ice minimum, while the position of the maximum winter ice margin is important for defining the highly productive MIZ (e.g. Wassmann et al., 2006). The advection of AW also contributes to longer productive seasons compared to other Arctic areas, making the Barents Sea one of the most productive areas of the Arctic Continental Shelf (Wassmann et al., 2006 and references cited therein).
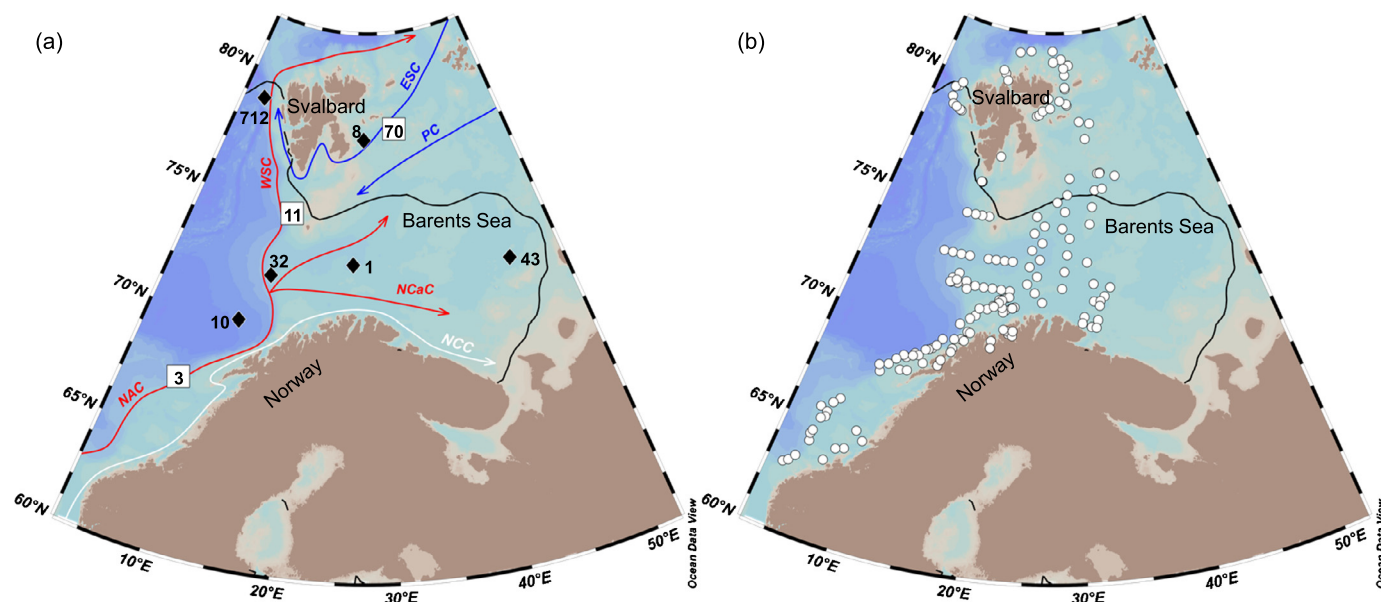
Fig. 2. Maps of the Barents Sea showing: (a) Labelled centennial (black diamonds) and millennial (white squares) downcore records, as well as a simplified representation of Atlantic Water, Arctic Water, and Coastal Water surface currents shown by red, blue, and white arrows, respectively. Abbreviations denote: WSC – West Spitsbergen Current; NAC – North Atlantic Current; NCaC – North Cape Current; NCC – Norwegian Coastal Current; ESC – East Spitsbergen Current; PC – Persey Current; (b) Surface sediment locations. For both maps, the solid black line illustrates the averaged (1988–2017) April–June sea ice extent, defined by a 15% SpSIC threshold. Maps were generated with Ocean Data View (http://odv.awi.de/). (For interpretation of the colours in the figure, the reader is referred to the web version of this article.)

3. Materials and methods

3.1. Surface sediment material

198 surface sediment sub-samples were taken from a range of grab samples, multicores, box cores and gravity cores reflecting regions of variable sea ice cover and seasonal primary productivity (Fig. 2b). All surface sediments are assumed to represent recent deposition, as described previously (Belt et al., 2015; Smik et al., 2016; Köseoğlu et al., 2018a and references therein). Sampling locations, core types, biomarker data and various physical parameters used for the calibration component of this study can be found in Supplementary Table 1.

3.2. Downcore sediment material

Downcore data spanning recent centuries were obtained from six short sediment cores (Fig. 2a) described in detail elsewhere (Vare et al., 2010; Dylmer, 2013; Cabedo-Sanz and Belt, 2016; Köseoğlu et al., 2018a). In brief, cores BASICC 1, BASICC 8, and BASICC 43, hereafter referred to as cores 1, 8, and 43, were recovered aboard the RV *Ivan Petrov* as part of the 'Barents Sea Ice Edge in a Changing Climate' (BASICC) project (Cochrane et al., 2009). We used the age models given elsewhere (Vare et al., 2010). Core MSM5/5-712-1 (hereafter, core 712) was collected aboard the RV *Maria S. Merian* during the MSM5/5 cruise and the age model is based on five ^{14}C Accelerated Mass Spectrometry (AMS) dates (Spielhagen et al., 2011). Multicores R248MC010 and R406MC032 (hereafter cores 10 and 32, respectively) were retrieved within the framework of the MAREANO programme (www.mareano.no) onboard F/F *G.O. Sars*, with chronologies based on ^{210}Pb data (see Dylmer, 2013 and references cited therein).

Longer timeframe data were obtained from gravity cores described previously (Laberg et al., 2002; Dylmer, 2013; Berben et al., 2014, 2017) (Fig. 2a). Gravity core WOO/SC-3 (hereafter core 3) was retrieved from the Norwegian continental margin (Laberg et al., 2002). The age model is based on three ^{14}C AMS dates (Laberg et al., 2002; Dylmer, 2013) and the analysed section corresponds to the last ca. 3.0 cal kyr BP. Core JM09-KA11-GC (hereafter, core

11), was obtained from the Kveithola Trough, south of Svalbard, aboard RV *Jan Mayen*. We use the age model presented in Belt et al. (2015), based on ^{14}C AMS dates from previous studies (Berben et al., 2014 and references therein). Gravity Core NP05-11-70GC (hereafter, core 70) was collected from the Olga Basin, East Svalbard, aboard the RV *Lance*. Core chronology is based on three ^{14}C AMS dates (Berben et al., 2017). For cores 11 and 70, we present data covering last ca. 9.5 cal. kyr BP. See Table 1 for a summary of all cores and Supplementary Table 2 for more details regarding core chronologies.

3.3. Biomarker data

Biomarker data were obtained in two ways. For cores not investigated previously (i.e. cores 3, 10 and 32), lipid analysis was carried out according to Belt et al. (2012), but with a slight modification to the extraction method. Thus, freeze-dried subsamples (ca. 1.5–2.5 g) were saponified in a methanolic KOH solution (ca. 5 mL H_2O:MeOH (1:9); 5% KOH) for 60 min (70 °C). Hexane (3 × 2 mL) was added to the saponified content, with non-saponifiable lipids (NSLs) transferred to clean vials and dried over N_2. NSLs were then re-suspended in hexane (0.5 mL) and fractionated using column chromatography (SiO_2; 0.5 g). Non-polar fractions containing HBIs were eluted with hexane (6 mL) and purified further using silver-ion chromatography (Belt et al., 2015). Saturated compounds were eluted with hexane (2 mL) and unsaturated compounds, including HBIs III and IV, were collected in a subsequent acetone fraction (3 mL). Prior to extraction, samples were spiked with an internal standard (9-octylheptadec-8-ene, 9-OHD, 10 μL; 10 μg mL^{-1}) to permit quantification. Analysis of purified fractions containing HBIs III and IV was carried out using gas chromatography–mass spectrometry (GC–MS) in total ion current (TIC) and selected ion monitoring (SIM) modes (Belt et al., 2012). HBIs were identified based on their characteristic GC retention indices (RI$_{HP5MS}$ = 2081, 2044 and 2091 for IP$_{25}$, HBI III and HBI IV, respectively) and mass spectra (Belt et al., 2000; Belt, 2018). HBI quantification was achieved by comparison of mass spectral responses of selected ions (e.g. IP$_{25}$, m/z 350; HBIs III and IV, m/z 346) in SIM mode with those of the internal

Table 1

Summary of core locations, water depths and age model methods for all the cores described in the study. Further information about the individual age models can be found in Supplementary Table 2.

Core ID	Short ID	Time interval	Latitude (°N)	Longitude (°E)	Water depth (m)	Age model method
R248MC010	10	Recent centuries	70.31	12.88	1254	^{210}Pb (Dylmer, 2013)
R406MC032	32	Recent centuries	72.32	15.38	1035	^{210}Pb (Dylmer, 2013)
BASICC 1	1	Recent centuries	73.10	25.63	425	^{210}Pb (Vare et al., 2010)
BASICC 8	8	Recent centuries	77.98	26.79	135	^{210}Pb (Vare et al., 2010)
BASICC 43	43	Recent centuries	72.54	45.74	285	^{210}Pb (Vare et al., 2010)
MSM5/5-712-1	712	Recent centuries	78.92	6.77	1491	^{14}C AMS (Spielhagen et al., 2011)
WOO/SC-3	3	Last ca. 3.0 kyr BP	67.40	8.52	1184	^{14}C AMS (Dylmer, 2013)
JM09-KA11-GC	11	Last ca. 9.5 kyr BP	74.87	16.48	345	^{14}C AMS (Belt et al., 2015)
NP05-11-70GC	70	Last ca. 9.5 kyr BP	78.40	32.42	293	^{14}C AMS (Berben et al., 2017)

standard (9-OHD, m/z 350) and normalized according to their respective instrumental response factors (Belt et al., 2012). For cores analysed previously, we used the data reported by Köseoğlu et al. (2018b). The proportions of the two tri-unsaturated HBIs (III and IV) in the form of an HBI triene ratio (HBI TR$_{25}$) and a re-arranged version of this (HBI T$_{25}$) were calculated according to Eqs. (1) and (2).

Biomarker-based spring sea ice concentration (%SpSIC) estimates (and their root-mean-square errors (RMSE)) were either obtained from the new biomarker data sets (i.e. for cores 3, 10 and 32) based on the relative concentrations of IP$_{25}$ and HBI III and a regional calibration (Eqs. (3) and (4); Smik et al., 2016), or have been reported previously using the same approach (Berben et al., 2017; Köseoğlu et al., 2018b). Square brackets denote absolute HBI concentrations (ng g^{-1} dry sed.). All downcore biomarker related data can be found in Supplementary Table 3.

$$HBI\,TR_{25} = \frac{[III]}{([III] + [IV])} \quad (1)$$

$$HBI\,T_{25} = \frac{HBI\,TR_{25}}{0.62} \quad (2)$$

$$P_{III}IP_{25} = \frac{[IP_{25}]}{([IP_{25}] + [III] \times 0.63)} \quad (3)$$

$$SpSIC(\%) = \frac{(P_{III}IP_{25} - 0.0692)}{0.0107} \quad (4)$$

3.4. Oceanographic data

Sea ice concentration data were obtained from Nimbus-7 SMMR and DMSP SSM/I-SSMIS databases on a 25 × 25 km grid (Cavalieri et al., 1996). Data from the Aqua satellite (NASA, https://oceancolor.gsfc.nasa.gov/data/aqua/) equipped with a Moderate Resolution Imaging Spectroradiometer (MODIS) was used to retrieve chlorophyll a (chl a; mg m^{-3}), particulate inorganic carbon (PIC; mol m^{-3}), photosynthetically available radiation (PAR; E m^{-2} d^{-1}), and sea surface temperatures (SST; °C). Sea surface salinity (SSS; psu; 0–30 m water depth) was obtained from World Ocean Atlas 2013 (https://www.nodc.noaa.gov/OC5/woa13/) on a 25 × 25 km grid. Monthly aggregates throughout April–August were created (chl a only), as well as those spanning April–June and July–September (all data). Daily-resolution chl a time series spanning 2003–2017 were also created to showcase differences between areas of contrasting spring (ca. April–June) phytoplankton productivity in the Barents Sea. Temporally-averaged (2003–2017) annual maximum concentration of chl a, and the timing of its occurrence (day of year), were also derived. The percentage differences between successive 8-daily averaged chl a (mg m^{-3}) spanning years 2003–2017 were calculated using Eq. (5), where Δchl a is the relative difference (in %) between an initial and subsequent

8-day chl a composite at the same location, labelled chl $a_{reference}$ and chl $a_{current}$, respectively.

$$\Delta chl\,a\,(\%) = \frac{(chl\,a_{current} - chl\,a_{reference})}{chl\,a_{reference}} \times 100 \quad (5)$$

3.5. Statistical analysis

To explore associations between the various datasets and between the HBI distributions and satellite-derived chl a data, in particular, Principal Component Analysis (PCA) and complete-linkage Agglomerative Hierarchical Clustering (AHC) using squared Euclidean distance were carried out using XLSTAT (Addinsoft, 2018). More specifically, PCA was used to reduce the high-dimensionality dataset of HBI concentrations, P$_{III}$IP$_{25}$, TR$_{25}$, satellite-derived and other variables in surface sediments for visualisation on a two-dimensional grid, where the proximity and magnitude of variables indicated their degree of association. Thus, satellite-derived parameters strongly associated with TR$_{25}$ according to PCA were chosen and individually processed via AHC to determine the optimal number and composition of clusters, as well as their similarity to those obtained using TR$_{25}$ data. The AHC helped determine a single satellite-derived parameter most closely associated with TR$_{25}$ in surface sediments.

4. Results

4.1. Distribution of HBIs III and IV in surface sediments

HBI IV could be quantified in virtually all surface sediments, consistent with the previous identification of near-ubiquity of HBI III in the same sediments (Köseoğlu et al., 2018a) and their co-production by certain marine diatoms (Rowland et al., 2001; Belt et al., 2000, 2017). The distributions of III and IV, when expressed as individual biomarker concentrations, were both somewhat heterogeneous (Fig. 3a, b); however, although spatial variability in the relative amounts of the two HBIs (i.e. HBI TR$_{25}$ (Eq. (1))) was also evident, generally higher values were observed for sites in the eastern region compared to those in the west (Fig. 3c).

Based on PCA (Fig. 4), we found no associations between the sedimentary concentrations of HBIs III or IV with any of the oceanographic parameters considered, including chl a. In contrast, HBI TR$_{25}$ exhibited a strong association with chl a, but mainly during April and May (i.e. during the spring phytoplankton bloom). AHC analysis between HBI TR$_{25}$ and chl a resulted in two clusters within areas of well-defined spring bloom seasonality and less productive regions characterised by strong Atlantic Water inflow and continuous upwelling (Fig. 5). Clustering was dependent on the month(s) selected for chl a data (i.e. April, May, April–May, April–June), with the April–May aggregate exhibiting the least mismatched cluster memberships ($n = 28$) relative to those of HBI TR$_{25}$ (Fig. 5). In contrast, the number of mis-matches for the other

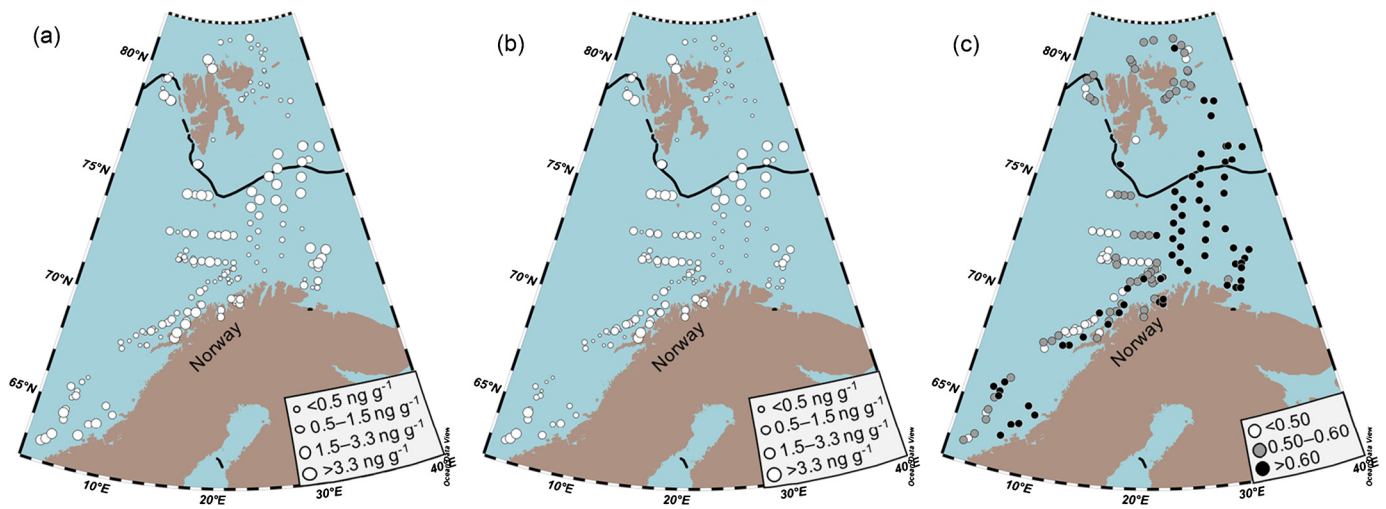**Fig. 3.** Distributions of absolute and relative HBI biomarker concentrations in Barents Sea surface sediments: (a) HBI III; (b) HBI IV; (c) HBI TR_{25}. The 15% SpSIC contour (1988–2017) is shown by a black line. Maps were generated with Ocean Data View (http:/odv.awi.de/). (For interpretation of the colours in the figure, the reader is referred to the web version of this article.)
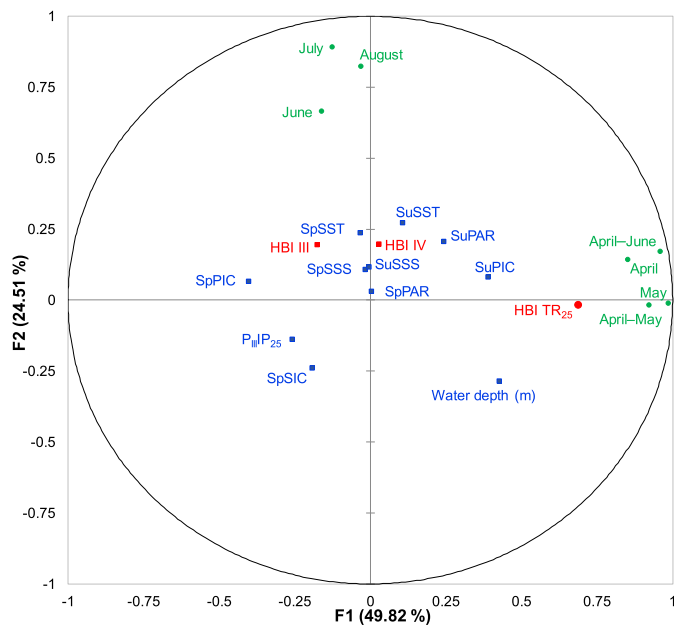

Fig. 4. Scaled factor loadings of primary (green markers) and secondary (blue markers) variables with HBI TR_{25} at surface sediment locations (Fig. 2b). Green labels denote months of averaged (2003–2017) satellite-derived chl a (mg m^{-3}). Blue labels represent surface sediment water depths (m), average (2003–2017) sea surface temperature (SST; °C), photoavailable radiation (PAR; E m^{-2} d^{-1}), particulate inorganic carbon (PIC; mol m^{-3}), 1955–2012 sea surface salinity (SSS; psu), as well as 1988–2017 sea ice concentration (SIC; %); prefixes "Su" and "Sp" denote summer (July–September) and spring (April–June). Absolute concentrations of III and IV (Fig. 1) and HBI TR_{25} are highlighted in red. (For interpretation of the colours in the figure, the reader is referred to the web version of this article.)

Fig. 5. Map of average chl a during April–May (2003–2017). Black and white circle markers represent the two AHC clusters of TR_{25} in surface sediments. Diagonal crosses denote HBI TR_{25} cluster memberships which mis-match those of the chl a data ($n = 28$). The 1.5 mg m^{-3} contour for chl a (2003–2017) is shown as a white line, and the 15% April–May sea ice concentration contour (1988–2017) is indicated by a black line. Maps were generated with Ocean Data View (http:/odv.awi.de/). (For interpretation of the colours in the figure, the reader is referred to the web version of this article.)

months ranged from 30 to 57 (Supplementary Fig. 1). Averaging the AHC centroids using the April–May aggregated chl a data yielded an approximate threshold value for HBI TR_{25} of ca. 0.62 $\pm$ 0.02 to separate regions of high (i.e. HBI $TR_{25} \geq 0.62$) and low (HBI $TR_{25} < 0.62$) April–May chl a delineated by a 1.5 mg m^{-3} boundary.

4.2. HBI biomarkers in downcore records

For cores representing recent centuries, the sea ice biomarker IP_{25} was absent (or below detection limits) in cores 1, 10 and 32 (Supplementary Fig. 2; Köseoğlu et al., 2018a) as expected
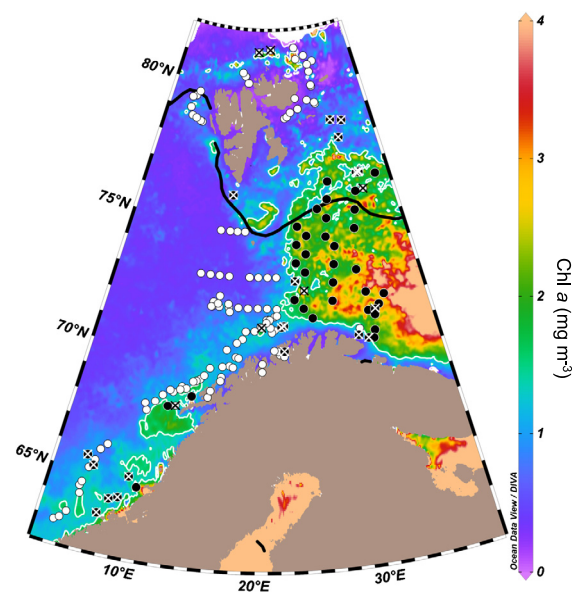
due to their ice-free settings in modern times (Fig. 2a). Further, HBIs III and IV were present in virtually all horizons in each core (with the exception of the early part of the record in core 32; Supplementary Fig. 2), consistent with our findings from proximal surface sediments described herein (Fig. 3a, b). In contrast, IP_{25} was identified in the three cores from sites of seasonal sea ice cover (i.e. cores 8, 43, 712; Vare et al., 2010; Cabedo-Sanz and Belt, 2016; Köseoğlu et al., 2018a), and HBIs III and IV were again present throughout, albeit in variable concentrations (Supplementary Fig. 2). HBI TR_{25} also exhibited some spatial variability, with values broadly reflecting those found in nearby surface sediments (Figs. 3c, 6a). Thus, relatively low (i.e. <0.62) HBI TR_{25} values were observed throughout each of cores 8, 10, 32 and 712, all of which are located in regions of low spring chl a in modern times. Similarly, consistently high HBI TR_{25} values (i.e.
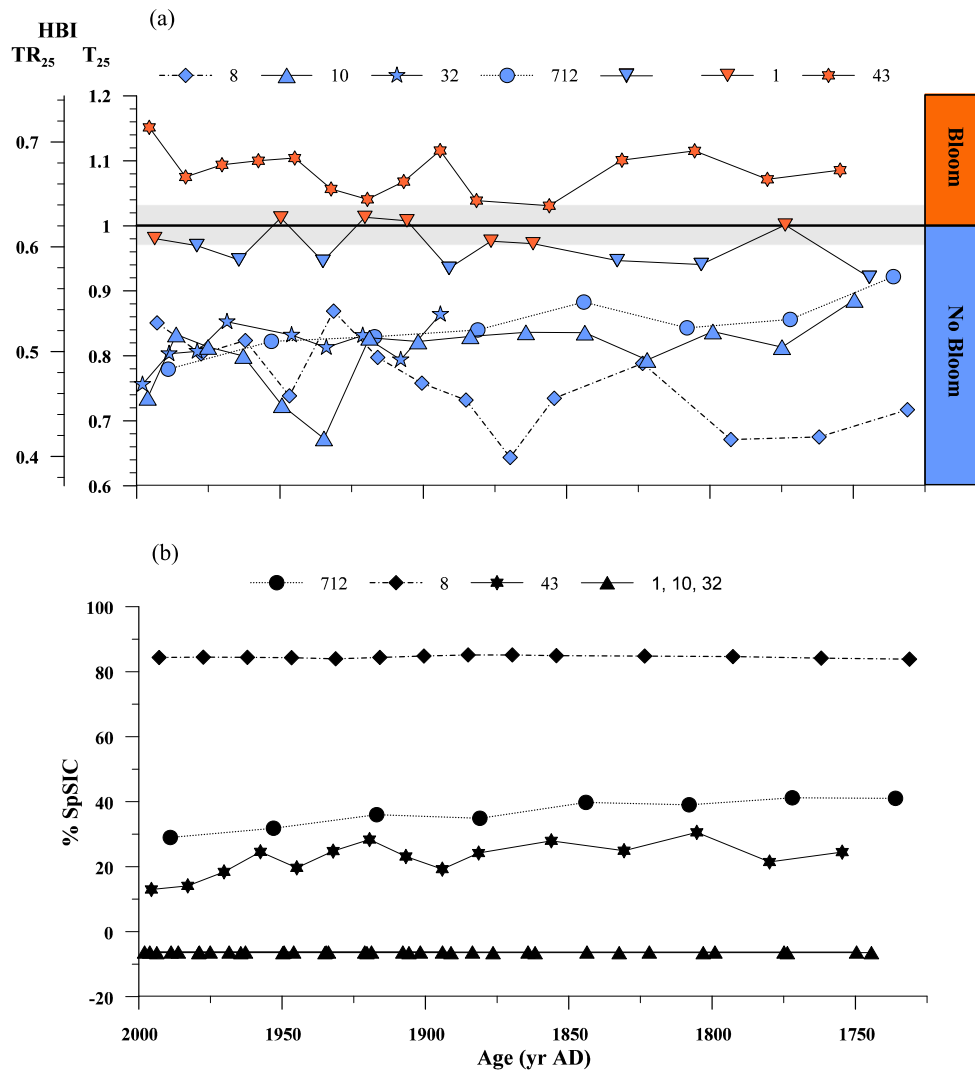
Fig. 6. HBI-derived proxy data from six short-core records within the study region, spanning recent centuries and experiencing contrasting sea ice and phytoplankton bloom occurrence in modern times: (a) HBI T_{25} and HBI TR_{25}. The binary threshold for the modern-day spring phytoplankton bloom (i.e. HBI $T_{25} > 1$) (Figs. 5, 9), is represented by a solid horizontal line. The shaded area represents the estimated error in this threshold (HBI TR_{25} ca. ± 0.02; HBI T_{25} ca. ± 0.03). The colours of each data point represent the proposed occurrence of a spring phytoplankton bloom (orange) versus no bloom (blue) at each core site/timeslice; (b) spring sea ice concentration estimates (% SpSIC). (For interpretation of the colours in the figure, the reader is referred to the web version of this article.)

>0.62) characterise core 43, located in a region of high spring chl *a* adjacent to the modern winter sea ice margin (Fig. 2a). In contrast, HBI TR_{25} values both above and below 0.62 were evident in core 1 (Fig. 6a).

In the longer timeframe records (i.e. cores 3, 11 and 70), individual biomarker concentrations and HBI TR_{25} values were also variable. For example, IP_{25} was not identified in core 3, although HBIs III and IV were present throughout the last ca. 3.0 cal kyr BP (Supplementary Fig. 3). Consistent with its low spring chl *a* setting in modern times, HBI TR_{25} was also <0.62 throughout (Fig. 7a). For core 11 IP_{25} and SpSIC were low during the early–mid Holocene, with increases in both to near-modern values since ca. 1.1 cal kyr BP, as reported previously (Berben et al., 2014; Belt et al., 2015) (Fig. 7b). HBI TR_{25} was low (<0.62) in the early Holocene, before increasing to ca. 0.62 around 6.0 cal kyr BP, and then to values consistently >0.62 after ca. 1.1 cal. kyr BP, coincident with increases to IP_{25} and SpSIC estimates (Fig. 7b). Finally, progressive increases to IP_{25} and SpSIC from the early to late Holocene characterise the core 70 site, as described previously (Belt et al., 2015; Berben et al., 2017) (Fig. 7c). HBIs III and IV were also present throughout the Holocene (Supplementary Fig. 3), with HBI TR_{25} values mainly greater than 0.62; however, slightly higher values

were observed ca. 9.0–6.0 cal kyr BP, while some values close to the 0.62 threshold were evident thereafter (Fig. 7c).

5. Discussion

5.1. Use of HBI TR_{25} and HBI T_{25} as proxies for the spring phytoplankton bloom

The spatially variable proportion of HBIs III and IV, albeit on a somewhat smaller sample set, was previously suggested to possibly reflect the spatial distribution of Atlantic Water (AW) and Arctic Water (ArW) in the region (Navarro-Rodriguez, 2014). The defining characteristics of both water masses include temperature and salinity (e.g. Loeng, 1991; Sakshaug et al., 2009). However, we observed no association between any of the spring-summer satellite sea surface temperature (SST), photoavailable radiation (PAR) or sea surface salinity (SSS) records and HBI TR_{25} in surface sediments presented herein (Fig. 4), which suggests the influence of these is either absent or obscured by competing effects. In contrast, chl *a* data, as an indicator of standing phytoplankton stocks, showed a strong correlation with HBI TR_{25}, but only during the spring bloom (i.e. April–May). This was further supported by simi-
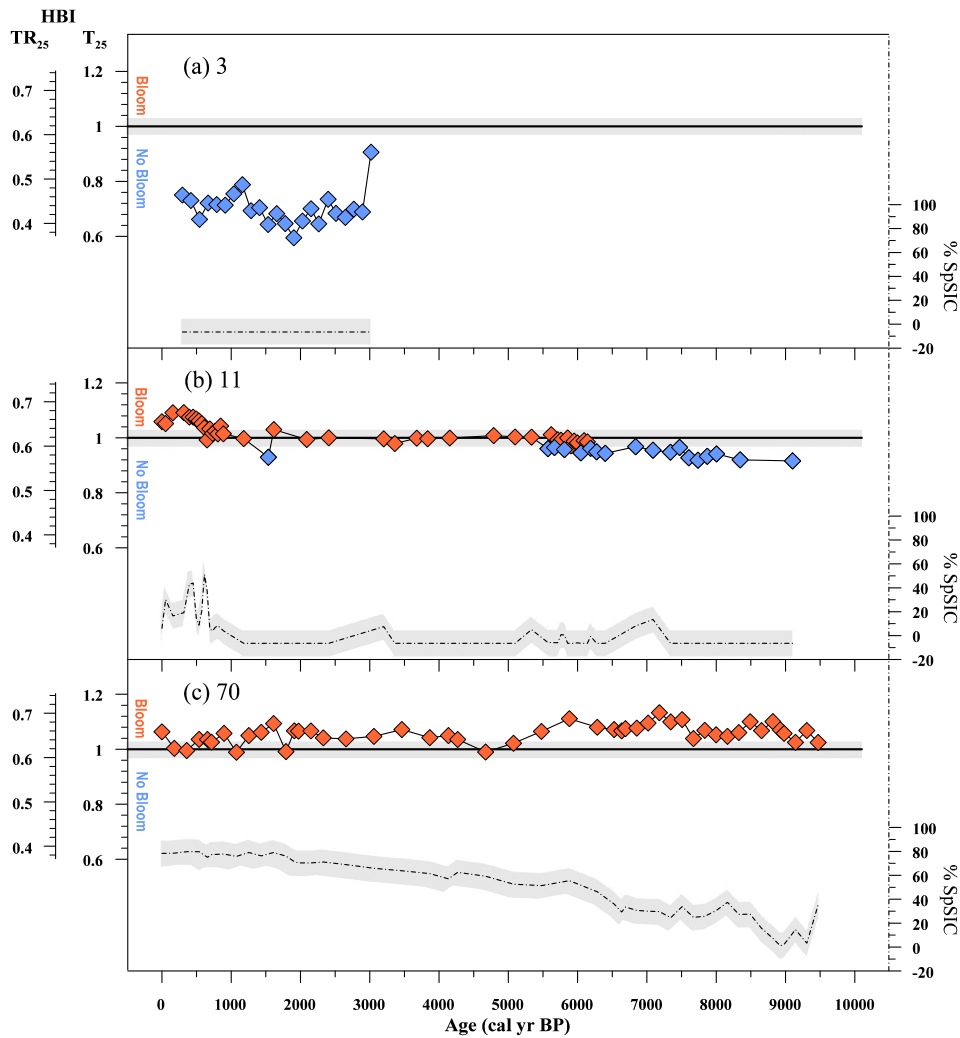
Fig. 7. HBI-derived proxy data for Holocene records: (a) 3; (b) 11; (c) 70. Left-hand axes: HBI TR$_{25}$ and HBI T$_{25}$ represented by solid line profiles with coloured markers. The solid horizontal line indicates the thresholds for the spring phytoplankton bloom (Figs. 5, 9), while the shaded area represents the estimated error in this threshold (HBI TR$_{25}$ ca. ±0.02; HBI T$_{25}$ ca. ±0.03). The colour of each data point represents the proposed occurrence of a spring phytoplankton bloom (orange) versus no bloom (blue) at each core site/timeslice. Right-hand axes: %SpSIC estimates represented by a dash-dotted line together with RMSE estimates (ca. ±11%; Smik et al., 2016). (For interpretation of the colours in the figure, the reader is referred to the web version of this article.)

lar clustering (AHC) of HBI TR$_{25}$ and chl *a* for April–May and (to a lesser extent) May only, likely due to the high spatio-temporal variability of phytoplankton bloom development in the Barents Sea.

Driven mainly by the spring phytoplankton bloom in April-May (Fig. 8a), maximum annual chl *a* (Fig. 8c) is highest on the highly-productive south-eastern and central shelves, reaching its maximum generally ca. 1–2 months earlier (Fig. 8d) compared to the western and northern Barents Sea (Fig. 8c). The highest rates of change in chl *a*, a further characteristic of a bloom event, are also most apparent along the south-eastern and central shelves (Fig. 8b). Along the western margin, slower (thermally-induced) vertical stratification and continuous AW upwelling hinder phytoplankton accumulation, while insufficient light penetration through thick ice cover lowers pelagic production at the northern margin (e.g. Dalpadado et al., 2014). Thus, in April, only the ice-free south-eastern Barents Sea shows significant increases in chl *a* (Supplementary Fig. 1a), followed by a propagation, north-eastwards along the retreating sea ice edge, by early May (Supplementary Fig. 1b). Phytoplankton biomass sharply declines by June (Fig. 8a) due to nutrient (e.g. nitrate and silicate) depletion and limited replenishment through the meltwater-established pycnocline in the marginal ice zone (MIZ) (e.g. Signorini and McClain, 2009;

Leu et al., 2011), with subsequent summer blooms dominated by coccolithophores (Hopkins et al., 2015), which are not HBI-producers.

Thus, HBI TR$_{25}$ appears to be most representative of the pelagic spring bloom throughout April–May. More specifically, HBI III is most prevalent (HBI TR$_{25}$ ≥ 0.62) in the eastern/central Barents Sea, where chl *a* is mainly in excess of 1.5 mg m^{-3}. In contrast, relatively increased IV (HBI TR$_{25}$ = ca. 0.4–0.45) generally occurs in the western Barents Sea, where chl *a* concentrations are generally in the range 0.5–1.5 mg m^{-3}. Furthermore, bloom seasonality is not as pronounced in the western Barents Sea compared to the eastern Barents Sea (Fig. 8a). Similarly, low HBI TR$_{25}$ is also evident in extensively ice-covered areas north and east of Svalbard, where the productive season is time- and nutrient-limited due to the late seasonal sea ice retreat throughout July–August (Signorini and McClain, 2009). This further supports our suggestion that HBI TR$_{25}$ is predominantly influenced by spring phytoplankton bloom development in the Barents Sea.

Finally, we suggest that the HBI TR$_{25}$ threshold for the spring phytoplankton bloom (i.e. HBI TR$_{25}$ ≥ 0.62) is most conveniently expressed as a simple binary measure using a slightly modified ratio of the two HBI trienes. Thus, HBI T$_{25}$ ≥ 1 (Eq. (2)) provides a proxy measure for the spring phytoplankton bloom (Fig. 9).
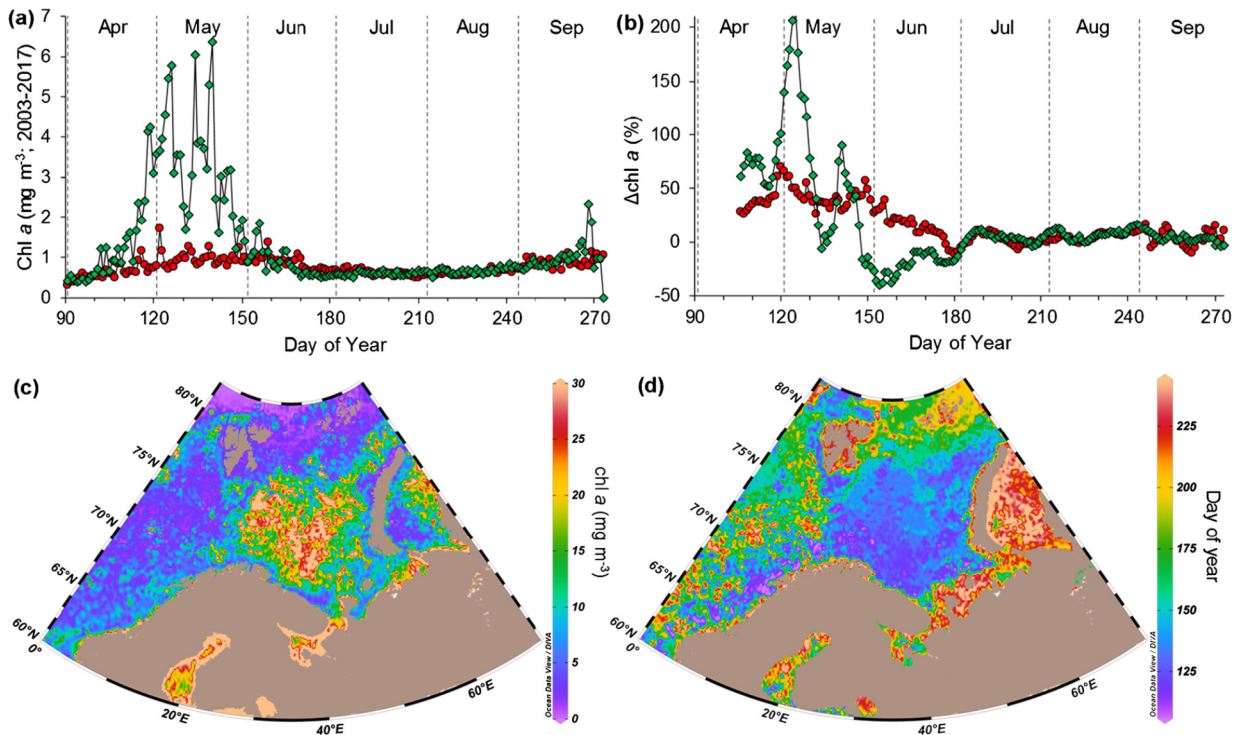
Fig. 8. Average (2003–2017) satellite-derived chl *a* data within the study area. Upper panel shows the temporal evolution of mean chl *a* for regions where there is a presence (green diamonds) or absence (red circles) of significant, diatom-dominated spring blooms according to a 1.5 mg m^{-3} April–May chl *a* threshold: (a) daily chl *a* concentration; (b) relative changes in chl *a*. Lower panel shows the temporally-averaged (2003–2017) annual chl *a* maximum (c) and the day of its maximum occurrence within the annual cycle (d). Maps were generated with Ocean Data View (http:/odv.awi.de/). (For interpretation of the colours in the figure, the reader is referred to the web version of this article.)
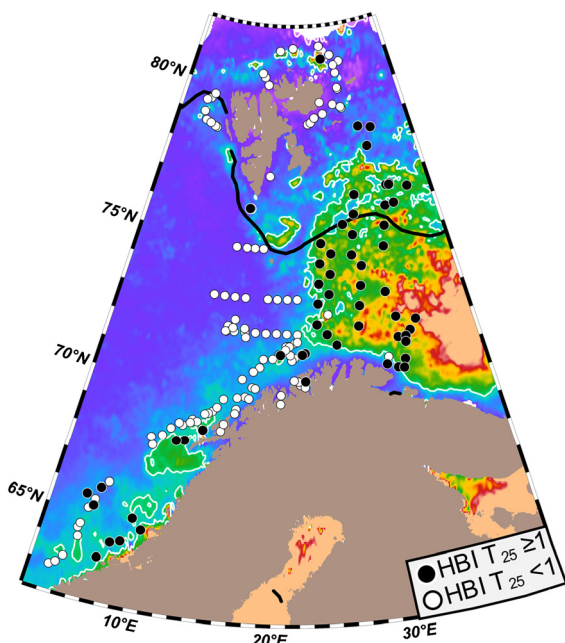

Fig. 9. Distribution of HBI T_{25} in surface sediments overlaid onto remotely-sensed April–May (2003–2017) chl *a*. The white line represents a 1.5 mg m^{-3} chl *a* contour and delimits zones of high and lower pelagic phytoplankton productivity during the spring bloom (Fig. 5c). Map was generated with Ocean Data View (http:/odv.awi.de/). (For interpretation of the colours in the figure, the reader is referred to the web version of this article.)

5.2. HBI TR_{25} and HBI T_{25} in records covering recent centuries

The HBI TR_{25} and HBI T_{25} data for the six short cores (i.e. 1, 8, 10, 32, 43 and 712) representing recent centuries reflect their

respective locations and the occurrence of spring phytoplankton blooms (or otherwise) within the modern context (note: we refer only to HBI T_{25} values from hereon). Thus, relatively low (<1) HBI T_{25} values prevail throughout the 10 and 32 records, consistent with low chl *a* at these ice-free locations (Figs. 2a, 6a).

Similarly, HBI T_{25} in core 712 was constantly below the threshold for a spring phytoplankton bloom. The core site is characterised by low chl *a* in modern times, and is located at the largely ice-free western Svalbard margin influenced by the strongest inflow of AW with the North Atlantic Current (NAC; Fig. 2). The contemporary ice edge duration at site 712 is limited, and stratification necessary for rapid spring bloom development is weaker due to continuous AW overturning (Smedsrud et al., 2013). However, instrumental records show that ice cover at the Svalbard margin was more extensive prior to ca. 1850 AD (Divine and Dick, 2006), supported by the $P_{III}IP_{25}$-based estimates of SpSIC reported previously (Fig. 6b; Cabedo-Sanz and Belt, 2016). Interestingly, a gradual decrease in HBI T_{25} at site 712, possibly indicative of a lower frequency of spring phytoplankton blooms, also coincides with the recent sea ice decline (Fig. 6a, b). Accordingly, increased phytoplankton stocks at site 712 prior to 1850 AD could be attributable to longer annual sea ice duration, when increased stratification potentially stabilised phytoplankton in the photic zone, facilitating the type of rapid growth normally associated with the contemporary MIZ in the central Barents Sea. Recent increases in AW inflow and atmospheric temperatures (e.g. Årthun et al., 2012) subsequently shifted the Barents Sea towards less productive, predominantly ice-free conditions dominated by continuous upwelling, with lower HBI T_{25} (Fig. 6a). Previously, Pathirana et al. (2015) also linked reduced MIZ duration in the Barents Sea to decreasing primary productivity over the last ca. 500 yr.

Core 8 exhibits similar HBI T_{25} values to core 712, but is located in a significantly different setting of increased (>80%) SpSIC north of the central Barents Sea MIZ, and influenced pre-

dominantly by colder ArW. HBI T_{25} values are, therefore, potentially attributable to reduced productivity in areas of prolonged seasonal sea ice duration, where the melt season is conversely shortened. Coupled with potential nutrient depletion within the surrounding waters as a consequence of rapid spring bloom development south of the core site (e.g. Wassmann et al., 2006; Signorini and McClain, 2009), the extensive sea ice cover at site 8 over recent centuries (Fig. 6b) likely prevented the development of spring phytoplankton blooms.

In contrast, cores 1 and 43 are characterised by consistently higher HBI T_{25} relative to cores 8, 10, 32 and 712 (Fig. 6a). In fact, the highest HBI T_{25} values in the current datasets are associated with core 43 (all HBI $T_{25} > 1$; Fig. 6a), a site located firmly within the spring phytoplankton bloom zone, with chl a values >2 mg m^{-3}. Spring productivity was likely enhanced by the consistent presence of a proximal ice edge with intermediate spring sea ice concentration (SpSIC) (Fig. 6b), which aided stratification during the melt season. Conversely, the absence of seasonal sea ice at site 1 may have reduced productivity somewhat, as indicated by slightly lower HBI T_{25} values (Fig. 6a). In fact, the somewhat oscillatory (either side of 1) pattern of HBI T_{25} likely reflects the close proximity of the core site to the recent (2003–2017) spring phytoplankton bloom boundary, with short-term variability over decadal (or shorter) timeframes during recent centuries. This possibly reflects the variable influence of the North Cape Current (NCaC), since intensified AW upwelling could have reduced the stability of the water column at the core site, resulting in lower productivity.

5.3. HBI T_{25} in Holocene records

In order to make a first assessment of the reliability of the HBI T_{25} proxy measure of the spring phytoplankton bloom over longer timeframes, we measured it in three early-late Holocene records from regions of contrasting sea ice and phytoplankton bloom occurrence in modern times, and for which evidence for temporal changes in oceanography had already been established from previous proxy-based investigations. The shortest of these records, obtained from core 3, located in the SW Barents Sea, adds to the findings presented earlier for sites 32 and 10 spanning recent centuries (Fig. 2a). Thus, consistently low HBI T_{25} in core 3 characterises this perennially ice-free region with low spring chl a over the last ca. 3.0 cal. kyr BP (Fig. 7a).

The core 11 site is proximal to the modern maximum winter sea ice margin (Fig. 2a). During the Holocene, HBI T_{25} gradually increased since ca. 9.5 cal kyr BP, with values generally exceeding the spring bloom threshold since the onset of the Neoglacial at ca. 6.0 cal kyr BP (Fig. 7b). According to previous investigations, the core 11 site was relatively ice-free during the Holocene (Berben et al., 2014; Belt et al., 2015); however, a highly-productive ice edge likely remained close to the Kveithola Trough following the Neoglacial ice advance, as previously suggested for Storfjorden (Knies et al., 2017), located slightly further north. High productivity fuelled by seasonal sea ice-induced stratification and AW upwelling could have propagated towards the core 11 site at ca. 6.0 cal kyr BP, thus promoting the occurrence of spring phytoplankton blooms as a more frequent feature. Finally, high (>1) HBI T_{25} in the late Holocene is consistent with spring phytoplankton blooms associated with the productive ice edge having reached the core site at ca. 1.1 cal kyr BP (Fig. 6b; Berben et al., 2014; Belt et al., 2015), a conclusion supported further by a productivity increase inferred from higher benthic foraminiferal content (Berben et al., 2014).

In contrast to cores 3 and 11, core 70 is situated at a site of extensive winter sea ice cover in modern times. However, conditions during the early Holocene were less severe, such that the site was proximal to the winter ice margin until ca. 6.0 cal kyr BP (SpSIC

ca. 20–50%; Fig. 7c) followed by a further progressive southward sea ice expansion and increase in SpSIC (Fig. 7c; Belt et al., 2015; Berben et al., 2017). Consistent with these changes, HBI T_{25} values are highest during the early–mid Holocene (up to ca. 6.0 cal. kyr BP), likely as a result of the favourable MIZ conditions, after which they undergo a slight decrease, possibly due to a reduction in the length of the open water season due to delayed sea ice retreat (cf. core 8). However, on the basis of HBI T_{25} values generally higher than 1 across the record, spring phytoplankton blooms would appear to have been an important feature of the core site throughout the record.

5.4. Rationalising the relationship between HBI T_{25} and spring phytoplankton blooms

Our surface sediment outcomes (PCA and cluster analyses), together with those from various downcore records suggest that the biomarker-based HBI T_{25} parameter described herein provides a qualitative proxy indicator for the occurrence of spring phytoplankton blooms across the study region from recent to Holocene timeframes. Intuitively, this association is perhaps not surprising given that HBIs are produced by the main constituents of the spring phytoplankton bloom (i.e. diatoms), although this alone does not provide adequate explanation for the observed relationship. For example, HBIs III and IV are present at virtually all study sites, irrespective of the occurrence (or not) of a spring phytoplankton bloom. Further, while absolute sedimentary concentrations of HBIs III and IV show a significant enhancement within the MIZ, they are relatively low in some other regions of high chl a (e.g. in the ice-free SE Barents Sea; Fig. 3) and are poorly associated with chl a (Fig. 4), more generally. The latter is potentially attributable to the increased prevalence of diatoms relative to other microalgae closer to the well-stratified waters near the ice edge (e.g. Wassmann et al., 2006; Sakshaug et al., 2009). Absolute biomarker concentrations are also influenced by sediment accumulation rates and export efficiency from the water column, both of which can be variable, spatially, and thus may not accurately reflect production, more generally. On the other hand, such influences are often much less important with ratio-based measures.

In any case, in order to rationalise the association between HBI T_{25} and the spring phytoplankton bloom, we briefly consider three possible contributing factors: (i) different sources of HBIs III and IV; (ii) differential biomarker degradation; (iii) variable phytoplankton growth rates.

First, HBIs III and IV are amongst the most common HBIs found in marine sediments (Belt et al., 2000), yet very few sources have been identified. Of these, *Rhizosolenia setigera* and related species are by far the most cosmopolitan and abundant, and HBIs III and IV have indeed been identified in such species from the current study region (Belt et al., 2017). In contrast, although HBIs III and IV have been reported in the benthic diatom *Pleurosigma intermedium* (Belt et al., 2000), they have not been identified in other marine *Pleurosigma* spp., which are, in any case, generally very low or absent in taxonomic inventories. The more common *Berkeleya rutilans* (Brown et al., 2014 and references cited therein) has been shown to produce HBI IV (but not HBI III) in culture, although we are not aware of any reports to indicate that the spatial distribution of *B. rutilans* (or *Rhizosolenia* spp.) would result in the variability of HBI T_{25} described herein. Likewise, additional contribution to sedimentary HBI IV may potentially also occur in ice covered regions since *B. rutilans* has been reported in sea ice (von Quillfeldt, 2000); however, this would result in a reduction in HBI T_{25} in such settings, which is not the case (Figs. 3, 9). Thus, we suggest that *R. setigera* and related species are likely to be the main sources of HBIs III and IV in the Barents Sea and neighbouring regions.

Of course, as yet unidentified sources of HBIs III and IV may also contribute to the observed sedimentary variability in HBI T_{25}, although some of the most common species characteristic of colder, nutrient-replete waters in the Barents Sea, such as *Thalassiosira* or *Fragilariopsis* spp. (von Quillfeldt, 2000), are not known to be HBI-producers.

Second, changes to HBI T_{25} may result from differential degradation of HBIs III and IV in the water column or sediments, or by selective removal through grazing. However, previous food web studies have shown no significant change to HBI composition prior to, and after, consumption (e.g. Brown and Belt, 2017; Schmidt et al., 2018). In some laboratory experiments, HBI IV was shown to be slightly more reactive than HBI III towards photo-oxidation and autoxidation (Rontani et al., 2014), although whether this is true under in situ environmental conditions is as yet unknown. In the meantime, we note that a higher rate of degradation of HBI IV would result in higher HBI T_{25} values for regions of increased water depth, yet the opposite is true in most cases. Further, we observe no significant association between HBI T_{25} and water depth in the PCA (Fig. 4).

Third, we consider whether variable HBI T_{25} is controlled by changes in growth rates of *R. setigera* (and potentially related *Rhizosolenia* spp.), with higher relative production of HBI III under conditions of more rapid growth (Fig. 8b). In support of this suggestion, Rowland et al. (2001) demonstrated a systematic increase in the amount of HBI III relative to HBI IV with increasing growth rate of *R. setigera* cultured at different temperatures. Since we observe no relationship between HBI T_{25} and SST in the current dataset, we therefore suggest that the variability described herein results from regional differences in phytoplankton growth rates (Fig. 8b). Such a working hypothesis will, of course, require testing through further investigations into the controls over HBI production by *R. setigera* and other HBI-producing diatoms, including laboratory-based studies and time-series monitoring of their production in the Barents Sea and other areas of well-defined primary productivity.

Increased growth rates of *R. setigera*, in particular, may also help explain some of the anomalies in our surface sediment data. For example, a number of mismatches in AHC cluster memberships of chl *a* and HBI T_{25} occurred along the south-western Barents and Norwegian Sea coastlines (Fig. 5), which could be a consequence of local effects associated with coastal water masses flowing inshore of the NAC and within the NCC. In such settings *R. setigera* has the potential to overtake other species under strong upwelling and nutrient-replete conditions, as seen at the western Svalbard shelf (Belt et al., 2017). Moreover, the NCC (Fig. 2a) carries brackish coastal waters from the Baltic Sea, where increasing dominance of *R. setigera* and other cold-water species during spring and early summer blooms has been reported (e.g. Wasmund et al., 2008). Interestingly, several of the higher HBI T_{25} values from near-coastal locations are also proximal to some chl *a* hotspots, despite the generally lower chl *a* for this region (Fig. 9).

Apart from the binary division between spring phytoplankton bloom (HBI $T_{25} > 1$) versus bloom-free (HBI $T_{25} < 1$) conditions (Fig. 9), we note some further variability in HBI T_{25} in both the surface sediment and downcore datasets (Figs. 6, 7) either side of this threshold. Such variability might potentially reflect the mean frequency (or intensity) of spring phytoplankton bloom occurrence at each site/timeslice, especially since the sediment horizons investigated herein (1-cm) typically represent ca. 20–50 yr of accumulation (e.g. Dylmer, 2013; Berben et al., 2014, 2017; Belt et al., 2015; Köseoğlu et al., 2018a). Such an interpretation would likely improve the value of the HBI T_{25} proxy in palaeo records beyond a simple binary measure, including the identification of temporal shifts in the frequency of spring phytoplankton blooms, more generally; however, this aspect also requires further investigation.

Finally, when used alongside IP$_{25}$ as a binary measure of seasonal sea ice (Belt, 2018) and PIP$_{25}$ as a semi-quantitative tool for spring sea ice concentration, the newly proposed HBI T_{25} proxy for the spring phytoplankton bloom has the potential to provide a more robust indicator of the MIZ in northern high latitude locations, and its spatial and temporal variation within the palaeo record.

6. Conclusions

Based on their distribution in surface sediments from across the Barents Sea and neighbouring regions, the relative amount of two tri-unsaturated HBI (III and IV; Fig. 1) lipids (HBI TR$_{25}$) appears to provide proxy evidence for the spring phytoplankton bloom. Further, by re-expressing the HBI TR$_{25}$ ratio in a simplified binary format, a threshold for the spring bloom is proposed (i.e. HBI $T_{25} \geq 1$). HBI T_{25} values in short (decadal-centennial) and long (Holocene) records from the region are consistent with the surface sediment calibration dataset, with some changes to the occurrence/frequency of the spring bloom linked to temporal changes in sea ice concentration identified previously. The identification of a novel proxy for the spring phytoplankton bloom for northern high latitudes (at least) could potentially provide important insights into characterising the marginal ice zone, especially when used alongside established sea ice proxies such as IP$_{25}$ and PIP$_{25}$.

Appendix A. Supplementary material

Supplementary material related to this article can be found online at https://doi.org/10.1016/j.epsl.2019.06.038.

References

Addinsoft, 2018. XLSTAT: Data Analysis and Statistical Solution for Microsoft Excel. Paris, France.

Arrigo, K.R., Perovich, D.K., Pickart, R.S., Brown, Z.W., van Dijken, G.L., Lowry, K.E., Mills, M.M., Palmer, M.A., Balch, W.M., Bahr, F., Bates, N.R., Benitez-Nelson, C., Bowler, B., Brownlee, E., Ehn, J.K., Frey, K.E., Garleym, R., Laney, S.R., Lubelczyk, L., Mathis, J., Matsuoka, A., Mitchell, B.G., Moore, G.W., Ortega-Retuerta, E., Pal, S., Polashenski, C.M., Reynolds, R.A., Schieber, B., Sosik, H.M., Stephens, M., Swift, J.H., 2012. Massive phytoplankton blooms under Arctic sea ice. Science 336, 1408.

Årthun, M., Eldevik, T., Smedsrud, L.H., Skagseth, Ø., Ingvaldsen, R.B., 2012. Quantifying the influence of Atlantic heat on Barents Sea ice variability and retreat. J. Climate 25, 4736–4743.

Bai, Y., Sicre, M.-A., Chen, J., Klein, V., Jin, H., Ren, J., Hongliang, L., Xue, B., Ji, Z., Zhuang, Y., Zhao, M., 2019. Seasonal and spatial variability of sea ice and phytoplankton biomarker flux in the Chukchi sea (western Arctic Ocean). Prog. Oceanogr. 171, 22–37.

Belt, S.T., 2018. Source-specific biomarkers as proxies for Arctic and Antarctic sea ice. Org. Geochem. 125, 277–298.

Belt, S.T., Allard, W.G., Massé, G., Robert, J.-M., Rowland, S.J., 2000. Highly branched isoprenoids (HBIs): identification of the most common and abundant sedimentary isomers. Geochim. Cosmochim. Acta 64, 3839–3851.

Belt, S.T., Brown, T.A., Navarro-Rodriguez, A., Cabedo-Sanz, P., Tonkin, A., Ingle, R., 2012. A reproducible method for the extraction, identification and quantification of the Arctic sea ice proxy IP$_{25}$ from marine sediments. Anal. Methods 4, 705–713.

Belt, S.T., Cabedo-Sanz, P., Smik, L., Navarro-Rodriguez, A., Berben, S.M.P., Knies, J., Husum, K., 2015. Identification of paleo Arctic winter sea ice limits and the marginal ice zone: optimised biomarker-based reconstructions of late Quaternary Arctic sea ice. Earth Planet. Sci. Lett. 431, 127–139.

Belt, S.T., Brown, T.A., Smik, L., Tatarek, A., Wiktor, J., Stowasser, G., Assmy, P., Allen, C.S., Husum, K., 2017. Identification of C$_{25}$ highly branched isoprenoid (HBI) alkenes in diatoms of the genus *Rhizosolenia* in polar and sub-polar marine phytoplankton. Org. Geochem. 110, 65–72.

Berben, S., Husum, K., Cabedo-Sanz, P., Belt, S., 2014. Holocene sub-centennial evolution of Atlantic water inflow and sea ice distribution in the western Barents Sea. Clim. Past 10, 181–198.

Berben, S.M.P., Husum, K., Navarro-Rodriguez, A., Belt, S.T., Aagaard-Sørensen, S., 2017. Semi-quantitative reconstruction of early to late Holocene spring and summer sea ice conditions in the northern Barents Sea. J. Quat. Sci. 32, 587–603.

Brown, T.A., Belt, S.T., Cabedo-Sanz, P., 2014. Identification of a novel di-unsaturated C$_{25}$ highly branched isoprenoid in the marine tube-dwelling diatom *Berkeleya rutilans*. Environ. Chem. Lett. 12, 455–460.

Brown, T.A., Belt, S.T., 2017. Biomarker-based H-Print quantifies the composition of mixed sympagic and pelagic algae consumed by *Artemia* sp. J. Exp. Mar. Biol. Ecol. 488, 32–37.

Cabedo-Sanz, P., Belt, S.T., 2016. Seasonal sea ice variability in eastern Fram Strait over the last 2000 years. Arktos 2, 22.

Cavalieri, D.J., Parkinson, C.L., Gloersen, P., Zwally, H.J., 1996. Sea Ice Concentrations from Nimbus-7 SMMR and DMSP SSM/I-SSMIS Passive Microwave Data, Version 1.1. NASA DAAC at the National Snow and Ice Data Center, Boulder, Colorado, USA (accessed 11.03.2019), updated yearly.

Cochrane, S.K.J., Denisenko, S.G., Renaud, P.E., Emblow, C.S., Ambrose Jr, W.G., Ellingsen, I.H., Skarðhamar, J., 2009. Benthic macrofauna and productivity regimes in the Barents Sea — ecological implications in a changing Arctic. J. Sea Res. 61, 222–233.

Dalpadado, P., Arrigo, K.R., Hjøllo, S.S., Rey, F., Ingvaldsen, R.B., Sperfeld, E., van Dijken, G.L., Stige, L.C., Olsen, A., Ottersen, G., 2014. Productivity in the Barents Sea – response to recent climate variability. PLoS ONE 9 (5), e95273.

Divine, D.V., Dick, C., 2006. Historical variability of sea ice edge position in the Nordic Seas. J. Geophys. Res., Oceans 111, C01001.

Dylmer, C., 2013. Late Holocene Surface Water Changes in the Eastern Nordic Seas: The Message from Carbonate and Organic-Walled Phytoplankton Microfossils. Ph.D. Thesis, University of Bordeaux.

Fetterer, F., Knowles, K., Meier, W.N., Savoie, M., 2016. Sea Ice Index. Ver. 2. NSIDC: National Snow and Ice Data Center, Boulder, Colorado [Digital Media, updated daily].

Hopkins, J., Henson, S.A., Painter, S.C., Tyrrell, T., Poulton, A.J., 2015. Phenological characteristics of global coccolithophore blooms. Glob. Biogeochem. Cycles 29, 239–253.

Knies, J., Pathirana, I., Cabedo-Sanz, P., Banica, A., Fabian, K., Rasmussen, T.L., Forwick, M., Belt, S.T., 2017. Sea-ice dynamics in an Arctic coastal polynya during the past 6500 years. Arktos 3, 1.

Köseoğlu, D., Belt, S.T., Husum, K., Knies, J., 2018a. An assessment of biomarker-based multivariate classification methods versus the PIP$_{25}$ index for paleo Arctic sea ice reconstruction. Org. Geochem. 125, 82–94.

Köseoğlu, D., Belt, S.T., Smik, L., Yao, H., Panieri, G., Knies, J., 2018b. Complementary biomarker-based methods for characterising Arctic sea ice conditions: a case study comparison between multivariate analysis and the PIP$_{25}$ index. Geochim. Cosmochim. Acta 222, 406–420.

Laberg, J.S., Vorren, T.O., Mienert, J., Bryn, P., Lien, R., 2002. The Trænadjupet Slide: a large slope failure affecting the continental margin of Norway 4,000 years ago. Geo Mar. Lett. 22, 19–24.

Legendre, L., 1990. The significance of microalgae blooms for fisheries and for the export of particulate organic carbon in oceans. J. Plankton Res. 12, 681–699.

Leu, E., Søreide, J.E., Hessen, D.O., Falk-Petersen, S., Berge, J., 2011. Consequences of changing sea-ice cover for primary and secondary producers in the European Arctic shelf seas: timing, quantity, and quality. Prog. Oceanogr. 90, 18–32.

Lind, S., Ingvaldsen, R.B., Furevik, T., 2018. Arctic warming hotspot in the northern Barents Sea linked to declining sea-ice import. Nat. Clim. Change 8, 634–639.

Loeng, H., 1991. Features of the physical oceanographic conditions of the Barents Sea. Polar Res. 10, 5–18.

Mahadevan, A., D'Asaro, E., Lee, C., Perry, M.-J., 2012. Eddy-driven stratification initiates North Atlantic spring phytoplankton blooms. Science 337, 54–58.

Müller, J., Wagner, A., Fahl, K., Stein, R., Prange, M., Lohmann, G., 2011. Towards quantitative sea ice reconstructions in the northern North Atlantic: a combined biomarker and numerical modelling approach. Earth Planet. Sci. Lett. 306, 137–148.

Navarro-Rodriguez, A., 2014. Reconstruction of Recent Palaeo Sea Ice Conditions in the Barents Sea. Ph.D. Thesis, Plymouth University.

Pathirana, I., Knies, J., Felix, M., Mann, U., Ellingsen, I., 2015. Middle to late Holocene paleoproductivity reconstructions for the western Barents Sea: a model-data comparison. Arktos 1, 20.

Polyak, L., Best, K.M., Crawford, K.A., Council, E.A., St-Onge, G., 2013. Quaternary history of sea ice in the western Arctic Ocean based on foraminifera. Quat. Sci. Rev. 79, 145–156.

Ragueneau, O., Tréguer, P., Leynaert, A., Anderson, R.F., Brzezinski, M.A., DeMaster, D.J., Dugdale, R.C., Dymond, J., Fisher, G., François, R., Heinze, C., Maier-Reimer, E., Martin-Jézéquel, V., Nelson, D.M., Quéguiner, B., 2000. A review of the Si cycle in the modern ocean: recent progress and missing gaps in the application of biogenic opal as a paleoproductivity proxy. Glob. Planet. Change 26, 317–365.

Renaut, S., Devred, E., Babin, M., 2018. Northward expansion and intensification of phytoplankton growth during the early ice-free season in Arctic. Geophys. Res. Lett. 45, 10590–10598.

Rontani, J.-F., Belt, S.T., Vaultier, F., Brown, T.A., Massé, G., 2014. Autoxidative and photooxidative reactivity of Highly Branched Isoprenoid (HBI) alkenes. Lipids 49, 481–494.

Rowland, S.J., Allard, W.G., Belt, S.T., Massé, G., Robert, J.M., Blackburn, S., Frampton, D., Revill, A.T., Volkman, J.K., 2001. Factors influencing the distributions of polyunsaturated terpenoids in the diatom, *Rhizosolenia setigera*. Phytochemistry 58, 717–728.

Sakshaug, E., Johnsen, G., Kristiansen, S., von Quillfeldt, C., Rey, F., Slagstad, D., Thingstad, F., 2009. Phytoplankton and primary production. In: Sakshaug, E., Johnsen, G., Kovacs, K. (Eds.), Ecosystem Barents Sea. Tapir Academic Press, Trondheim, pp. 167–208.

Schmidt, K., Brown, T.A., Belt, S.T., Ireland, L.C., Taylor, K.W.R., Thorpe, S.E., Ward, P., Atkinson, A., 2018. Do pelagic grazers benefit from sea ice? Insights from the Antarctic sea ice proxy IPSO$_{25}$. Biogeosciences 15, 1987–2006.

Seidenkrantz, M.-S., 2013. Benthic foraminifera as palaeo sea-ice indicators in the subarctic realm – examples from the Labrador Sea–Baffin Bay region. Quat. Sci. Rev. 79, 135–144.

Smedsrud, L.H., Esau, I., Ingvaldsen, R.B., Eldevik, T., Haugan, P.M., Li, C., Lien, V.S., Olsen, A., Omar, A.M., Otterå, O.H., Risebrobakken, B., Sandø, A.B., Semenov, V.A., Sorokina, S.A., 2013. The role of the Barents Sea in the Arctic climate system. Rev. Geophys. 51, 415–449.

Smik, L., Cabedo-Sanz, P., Belt, S.T., 2016. Semi-quantitative estimates of paleo Arctic sea ice concentration based on source-specific highly branched isoprenoid alkenes: a further development of the PIP$_{25}$ index. Org. Geochem. 92, 63–69.

Signorini, S.R., McClain, C.R., 2009. Environmental factors controlling the Barents Sea spring-summer phytoplankton blooms. Geophys. Res. Lett. 36, L10604.

Søreide, J.E., Leu, E., Berge, J., Graeve, M., Falk-Petersen, S., 2010. Timing of blooms, algal food quality and *Calanus glacialis* reproduction and growth in a changing Arctic. Glob. Change Biol. 16, 3154–3163.

Spielhagen, R.F., Werner, K., Sørensen, S.A., Zamelczyk, K., Kandiano, E.S., Budéus, G., Husum, K., Marchitto, T.M., Hald, M., 2011. Enhanced modern heat transfer to the Arctic by warm Atlantic Water. Science 331, 450–453.

Vare, L.L., Massé, G., Belt, S.T., 2010. A biomarker-based reconstruction of sea ice conditions for the Barents Sea in recent centuries. Holocene 40, 637–643.

von Quillfeldt, C.H., 2000. Common diatom species in Arctic spring blooms: their distribution and abundance. Bot. Mar. 43, 499–516.

Wasmund, N., Göbel, J., Bodungen, B.v., 2008. 100-years-changes in the phytoplankton community of Kiel Bight (Baltic Sea). J. Mar. Syst. 73, 300–322.

Wassmann, P., Reigstad, M., Haug, T., Rudels, B., Carroll, M.L., Hop, H., Gabrielsen, G.W., Falk-Petersen, S., Denisenko, S.G., Arashkevich, E., Slagstad, D., Pavlova, O., 2006. Food webs and carbon flux in the Barents Sea. Prog. Oceanogr. 71, 232–287.